Journal of
Materials Chemistry

Cite this: *J. Mater. Chem.*, 2012, **22**, 8399

www.rsc.org/materials

PAPER

Indolo[3,2-*b*]carbazole/benzimidazole hybrid bipolar host materials for highly efficient red, yellow, and green phosphorescent organic light emitting diodes†

Hao-Chun Ting,[a] You-Ming Chen,[a] Hong-Wei You,[b] Wen-Yi Hung,*[b] Sheng-Hsun Lin,[c] Atul Chaskar,[a] Shu-Hua Chou,[a] Yun Chi,[c] Rai-Hsung Liu*[c] and Ken-Tsung Wong*[a]

Received 12th January 2012, Accepted 13th February 2012
DOI: 10.1039/c2jm30207a

By incorporating electron-accepting benzimidazole and electron-donating indolo[3,2-*b*]carbazole into one molecule, two novel donor–acceptor bipolar host materials, **TICCBI** and **TICNBI**, have been synthesized. The photophysical and electrochemical properties of the hybrids can be tuned through the different linkages (C- or N-connectivity) between the electronic donor and acceptor components. The promising physical properties of these two new compounds made them suitable for use as hosts doped with various Ir or Os-based phosphors for realizing highly efficient phosphorescent organic light emitting diodes (PhOLEDs). PhOLEDs using **TICCBI** and **TICNBI** as hosts incorporated with Ir-based emitters such as green $(PPy)_2Ir(acac)$, yellow $(Bt)_2Ir(acac)$, and two new red emitters $(35dmPh\text{-}6Fiq)_2Ir(acac)$ (**i3**) and $(4t\text{BuPh-}6\text{Fiq})_2\text{Ir(acac)}$ (**i6**) accomplished high external quantum efficiencies ranging from 14 to 16.2%. Nevertheless, the red PhOLED device incorporating **TICNBI** doped with the red emitter osmium(II) bis[3-(trifluoromethyl)-5-(4-*tert*-butylpyridyl)-1,2,4-triazolate] dimethylphenylphosphine $[Os(bpftz)_2(PPhMe_2)_2]$ achieved a maximum external quantum efficiency, current efficiency, and power efficiency of 22%, 28 cd A^{-1}, and 22.1 lm W^{-1}, respectively, with CIE coordinates of (0.65,0.35). The external quantum efficiency remained high (20%) as the brightness reached to 1000 cd m^{-2}, suggesting balanced charge fluxes within the emitting layer, rendering devices with limited efficiency roll-off.

1. Introduction

Organic light-emitting diodes (OLEDs) have aroused considerable interest because of their potential applications in low power consumption displays, lighting and the printed electronics industry.[1] More importantly, 100% internal quantum efficiency can be achieved by dispersing appropriate transition metal-centered phosphorescent dopant in a suitable host material which can harvest both electron-generated singlet and triplet excitons.[2] The selection of host material for the phosphorescent dopant is one of the key factors in the design of next generation highly efficient phosphorescent organic light-emitting diodes (PhOLEDs). The host material must possess the ability to suppress the pernicious effects such as aggregation quenching and triplet–triplet annihilation of phosphorescent emitters.[3] Nevertheless, poor carrier mobility and unbalanced charges in the emitting layer have been observed to hamper the power efficiency of OLEDs.[4] The host materials should cope with some intrinsic properties like higher triplet energies than that of the phosphorescent emitter,[5] balanced charge flux, appropriate energy levels aligned with the neighboring functional layers[6] and good thermal and morphological stabilities. In the initial endeavours of PhOLED research, the unipolar hosts, namely, hole-transporting material consisting electron-donating moiety and electron-transporting material possessing electron-withdrawing moiety have been employed. The unbalanced charge flux of using unipolar hosts which shifts the recombination zone near to HTL or ETL, leading to a narrow charge recombination zone, resulted in possible triplet–triplet annihilation and exciton diffusion. The main objective of the present PhOLED research is the development of tailor-made bipolar host materials by proper selection and linking of hole- and electron-transporting moieties which could promote balanced charge density for the supply of balanced flux of electrons and holes to electroluminescent (EL) materials, leading to the realization of highly efficient PhOLEDs. So far, numerous classes of bipolar host materials have been reported which comprise triaryl amine or carbazole moieties as hole-transporting group and oxadiazole, triazole, azine, phenanthroline, benzimidazole, *etc.*, as electron-transporting

---

[a]*Department of Chemistry, National Taiwan University, Taipei 106, Taiwan. E-mail: kenwong@ntu.edu.tw; Fax: +886-2-33661667; Tel: +886-2-33661665*
[b]*Institute of Optoelectronic Sciences, National Taiwan Ocean University, Keelung 202, Taiwan. E-mail: wenhung@mail.ntou.edu.tw*
[c]*Department of Chemistry, National Tsing Hua University, Hsinchu 300, Taiwan*

† Electronic supplementary information (ESI) available: Experimental procedure, spectral analysis, crystal data, AFM images of **TICCBI** and **TICNBI**, and DFT calculation. CCDC reference numbers 864064, 864065. For ESI and crystallographic data in CIF or other electronic format see DOI: 10.1039/c2jm30207a

group.[7] More recently, Ma and Yang *et al.* reported universal bipolar hosts incorporating benzimidazole/aryl amine hybrid for hosting blue, green, orange and white phosphors, achieving maximum external quantum efficiencies (η_{ext}) of 16.1%, 22.7%, 20.5% and 19.1%, respectively.[8] In addition, PhOLEDs utilizing a carbazole/phosphine oxide hybrid bipolar host material BCPO reported by Cheng and Chou exhibited significantly promising efficiencies of 23.5%, 21.6% and 17% for blue, green, and red, respectively.[9] We have also used benzimidazole/carbazole hybrid to realize highly efficient yellow-green PhOLED with the η_{ext} of 19.2% and power efficiency of 62 lm W^{-1}.[10]

Among the bipolar host materials reported in the literature, we found that they are associated with low electrochemical stability due to the easily polymerized hole-transporting moieties such as triaryl amine/carbazole.[11] Taking into account this observation, we envision that still there is ample scope to develop the novel bipolar host using electrochemically stable hole-transporting moiety. Comparing with carbazole, indolo[3,2-*b*]carbazole derivatives also demonstrate great hole-transporting ability[12] and have been applied in various organic electronics such as hole-transporting material in light-emitting diodes,[13] transistors,[14] and photovoltaic cells.[15] However, to the best of our knowledge, indolo[3,2-*b*]carbazole has been seldom reported as the host material in OLEDs.[16] In the quest for novel bipolar host, we show here for the first time that the combination of indolo[3,2-*b*]carbazole as donor and benzimidazole moieties as acceptor in designing of new bipolar host materials **TICCBI** and **TICNBI** (Scheme 1) can lead to thermal and morphological stabilities, bipolar transporting characteristics and suitable triplet energy (E_T), consequently enhance the efficiency of PhOLEDs. By changing the linking topologies between the donor and acceptor, we are able to manipulate the spatial distributions of molecular orbital distributions locating at the different structural features to modulate the photophysical and electrochemical properties.

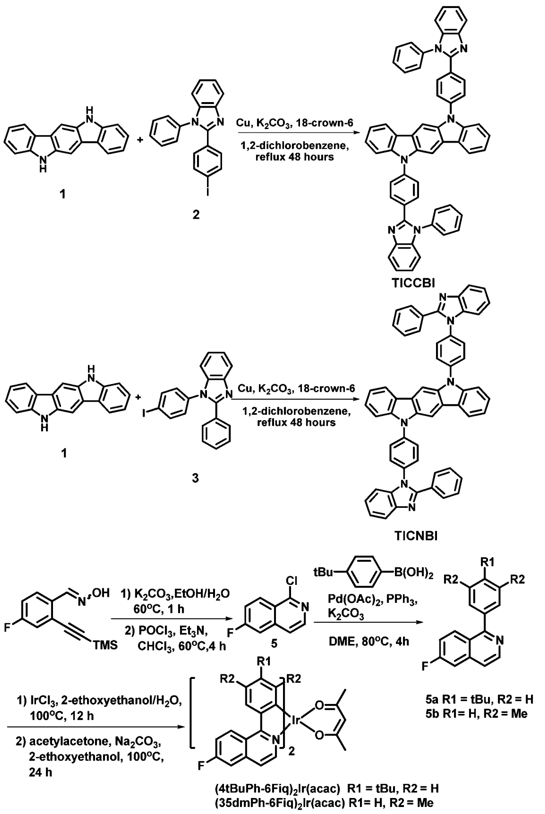

Scheme 1 Synthetic routes and chemical structures of **TICCBI**, **TICNBI**, bipolar hosts and (4*t*BuPh-6Fiq)$_2$Ir(acac), (35dmPh-6Fiq)$_2$Ir(acac) emitters.

Along with these two bipolar hosts we also reported the synthesis of two new red Ir complexes. It is well known that (piq)$_2$Ir(acac) derivatives,[17] where piq is 1-(phenyl)isoquinoline, can efficiently suppress the triplet–triplet annihilation showing short phosphorescent lifetime (~1.2 to 2.5 μs). According to DuPont group's theories[18] and previous literature,[19] the introduction of various substituents (*e.g.* *t*Bu, F, Me, OMe) on Ir-complexes can not only alter the HOMO–LUMO levels and emission wavelength but also minimize molecular packing and concentration quenching of luminescence. For better utilizing the advantages of chemical structure tuning, we tried to attach bulkyl and halo-substituent like F, *t*-Bu and Me on Ir-phenylisoquinolino complexes to reduce the self-quenching effect which is believed to cause low device efficiency. Among the substituted phenylisoquinoline-based iridium complexes, the complexes associated with (4*t*BuPh-6Fiq)$_2$Ir(acac) (**i6**) and (35dmPh-6Fiq)$_2$Ir(acac) (**i3**) derivatives of isoquinoline ligand show suitable photoluminescence wavelength in dichloromethane (618 nm and 628 nm, respectively).

This study focuses on the tuning of the thermal, photophysical and electrical properties by different linking topologies between the donor and acceptor constituents, synthesis of new Ir-based phosphors ((35dmPh-6Fiq)$_2$Ir(acac) and (4*t*BuPh-6Fiq)$_2$Ir(acac)) as well as the performance of PhOLEDs hosted by **TICCBI** and **TICNBI**. Green devices hosted by **TICCBI** and **TICNBI** along with (PPy)$_2$Ir(acac) emitter have efficiency values of 14% and 15%, respectively. While, the yellow devices of the same hosts with (Bt)$_2$Ir(acac) emitter reveal efficiency of 15.4% and 16.2%. The red PhOLEDs of these hosts show efficiency values of 14.4% and 15.6% in conjugation with (35dmPh-6Fiq)$_2$Ir(acac) emitter whereas the values are 15.3% and 15.5% for (4*t*BuPh-6Fiq)$_2$Ir(acac) emitter. Noteworthily, the device adopting **TICNBI** as the host and Os(bpftz)$_2$(PPhMe$_2$)$_2$ as the emitter provided a saturated red electrophosphorescence with CIE coordinates (*x*,*y*) of (0.65,0.35) and remarkably high efficiencies of 22% (28 cd A^{-1}) and 22.1 lm W^{-1}.

2. Results and discussion

2.1 Synthesis

Scheme 1 depicts the synthesis of two indolo[3,2-*b*]carbazole-cored bipolar host materials **TICCBI** and **TICNBI**, and two red Ir-centered phosphors (35dmPh-6Fiq)$_2$Ir(acac) and (4*t*BuPh-6Fiq)$_2$Ir(acac). **TICCBI** and **TICNBI** were readily prepared by Ullmann coupling reaction of indolo[3,2-*b*]carbazole[20] with 2-(4-iodophenyl)-1-phenyl benzimidazole (**2**) and 1-(4-iodophenyl)-2-phenyl benzimidazole (**3**),[21] respectively. The red emitters (35dmPh-6Fiq)$_2$Ir(acac) and (4*t*BuPh-6Fiq)$_2$Ir(acac) are synthesised from 4-fluoro-2-((trimethyl silyl) ethynyl) benzaldehyde oxime. The cyclization followed by Suzuki coupling with substituted phenyl boronic acid yielded **5b** and **5a** which on further reaction with iridium trichloride and acetyl acetone offered $(35dmPh\text{-}6Fiq)_2Ir(acac)$ and $(4t\text{BuPh-}6Fiq)_2Ir(acac)$, respectively. The products were purified by column chromatography and further purification was carried out by sublimation. ^{1}H and ^{13}C NMR spectra, mass spectral data (FAB and HRMS), and elemental analysis of **TICCBI**, **TICNBI**, $(35dmPh\text{-}6Fiq)_2Ir(acac)$ and $(4t\text{BuPh-}6Fiq)_2Ir(acac)$ are in agreement with the structural identities and purities.

2.2 Thermal analysis

TICCBI and **TICNBI** exhibited excellent morphological stabilities with distinct glass transition temperatures (T_g) of 174 °C and 168 °C and melting points (T_m) of 385 °C and 406 °C respectively, determined by using differential scanning calorimetry (DSC). **TICCBI** and **TICNBI** also showed to have high heat tolerance with decomposition temperatures (T_d) of 466 °C for **TICCBI** and 475 °C for **TICNBI**, corresponding to 5% weight loss, which were determined by using thermogravimetric analysis (TGA). The data are summarized in Table 1. Furthermore, these compounds exhibit very good film stability as investigated by atomic force microscopy (AFM). As shown in Fig. S4 in the ESI†, the homogeneous films showed very smooth surface upon annealing at 100 °C for 30 min under nitrogen, giving a root-mean-square (RMS) roughness of 0.279 nm for **TICCBI**, and 0.339 nm for **TICNBI** film. The rigid molecular configuration of **TICCBI** and **TICNBI** enhances their thermal and morphological stabilities. These morphological and thermal stabilities are desirable for the host material in PhOLEDs as they can suppress the aggregation formation and render amorphous characteristics in the solid film state.

2.3 Photophysical properties

Fig. 1 displays electronic absorption (UV-vis) and photoluminescence (PL) spectra (recorded at room temperature) of **TICCBI** and **TICNBI** in various solutions and in the form of solid thin films, as well as their phosphorescence spectra in EtOH at 77 K; Table 1 summarizes the data. In the UV-vis spectra of **TICCBI** and **TICNBI**, the solvent polarity independent absorption peaks from 330 to 340 nm are ascribed to the π–π* transition and peaks around 400 nm are owing to n–π* transition of the indolocarbazole moiety. In addition, we observed a broad peak from 350 to 380 nm as the charge transfer absorption in **TICCBI**. While the π–π* absorption spectra of **TICCBI** and **TICNBI** thin films centered at 345 and 344 nm, respectively, were slightly red-shifted relative to those of solutions (Fig. 1). Since bipolar molecules **TICCBI** and **TICNBI** are composed of indolocarbazole as the central donor and phenyl benzimidazole as the peripheral acceptors, it is reasonable to anticipate the occurrence of intramolecular charge transfer. Therefore, in order to explore the charge transfer phenomenon in the ground state and excited state, we have measured the UV-vis and PL spectra of **TICCBI** and **TICNBI** in various organic solvents. The absorption spectra of these two molecules in cyclohexane, toluene, dichloromethane and acetonitrile are nearly identical. The solvent-independent absorption spectra indicate that the Franck–Condon transitions are subjected to rather small dipole moment change in the ground state.[22] In contrast, significant solvent-dependent PL emission spectra of **TICCBI** were observed, showing different behaviour of the excited state as compared to those of **TICNBI**. The short wavelength region around 410 nm with distinct vibronic features stays intact while the long wavelength tailing of the emission spectra shifts continuously along with the solvent polarity, indicating fluorescence solvatochromism in **TICCBI**. This result suggests the generation of a highly polar charge-separated excited state of **TICCBI** due to D–A charge transfer upon excitation, giving the PL highly sensitive to the dielectric environment. In contrast, **TICNBI** only displayed solvent-independent emission with locally excited emission from donor moiety (indolocarbazole). The neat films' PL spectra of **TICCBI** and **TICNBI** were red-shifted by 5–10 nm as compared to those in CH_2Cl_2 solution (Fig. S1 in the ESI†), revealing different dielectric surrounding in the solid state, which is usually encountered in typical organic solids. Apparently, a stronger charge transfer emission peak centered at 450 nm was detected for the thin film of **TICCBI**. Notably, the triplet energies (E_T) of **TICCBI** and **TICNBI**, determined from the highest energy peaks of the phosphorescence spectra, are identical as 2.61 eV. The values of E_T of **TICCBI** and **TICNBI** are sufficiently high for them to host the green, yellow, and red phosphorescent emitters.

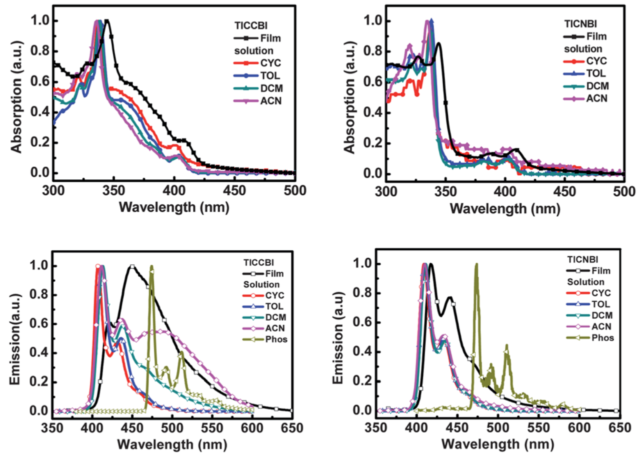

Fig. 1 Room-temperature UV-vis and PL spectra of **TICCBI** and **TICNBI** in various solutions and in neat films, as well as phosphorescence (Phos.) spectra recorded from their EtOH solutions at 77 K.

Table 1 Physical properties of **TICCBI** and **TICNBI**

	$(T_g/T_m/T_d)$/°C	$(E_{1/2}^{\mathrm{Ox}a}/E_{1/2}^{\mathrm{Red}b})$/V	λ_{abs} sol^c/nm	λ_{abs} film/nm	λ_{PL} sol^c/nm	λ_{PL} film/nm	E_T/eV	(HOMO/LUMO/E_g^d)/eV
TICCBI	174/385/466	0.48/−2.63	277 338 405	279 345 409	413 439	420 449	2.61	−5.3/−2.3/3.0
TICNBI	168/406/475	0.51/—	268 337 401	270 344 409	411 435	418 441	2.61	−5.5/−2.5/3.0

[a] In CH_2Cl_2 containing 0.1 M $TBAPF_6$. [b] In DMF containing 0.1 M TBAP. [c] In CH_2Cl_2. [d] Determined through AC-2 measurements; LUMO = HOMO+ E_g; the value of E_g was calculated from the absorption onset of the solid film.

2.4 Theoretical study

Quantum mechanical calculations were further conducted to understand the interesting photophysical properties of **TICCBI** and **TICNBI** at the molecular level using the GAUSSIAN 09 suite program. We try to characterize the first singlet excited states (S_1), aiming at realizing the geometries and molecular-orbital contributions for the fluorescent electronic transitions.[23] The calculations of excited-state properties significantly require more computational efforts than needed for the ground state. To reach this goal, most quantum-mechanical excited-state studies employ the configuration interaction with all singly excited determinants (CIS)[24] as a cost-effective approach for optimizing the S_1 structures. Geometry optimizations of singlet ground states (S_0) and the HOMO/LUMO orbitals for **TICCBI** and **TICNBI** were processed by density functional theory (DFT) using Beck's three-parameterized Lee–Yang–Parr exchange functional (B3LYP) with 6-31G(d) basis sets as shown in Fig. 2. The HOMO orbitals are mostly distributed over the indolocarbazole unit of **TICCBI** and **TICNBI**. In addition, the phenylene linker between the donor and acceptor units also contributes to the HOMO orbitals. This indicates that the HOMO levels of **TICCBI** and **TICNBI** are mainly determined by the indolocarbazole and phenylene linker with considerable contribution from the former. Particularly noteworthy, the LUMO orbital of **TICNBI** is located on indolocarbazole, whereas the LUMO of **TICCBI** is dispersed on whole phenyl benzimidazole moiety. The complete spatial separation of HOMO and LUMO energy levels in **TICCBI** suggests that the HOMO–LUMO excitation would shift the electron density distribution from the central indolocarbazole to the peripheral phenyl benzimidazole moieties, leading to a polarized excited state which supports our observation of red-shift emission in polar solvents.

In order to predict the excited states, optimized ground state geometries of **TICCBI** and **TICNBI** were optimized in the S_1 by CIS methods with 6-31G(d) basis sets. After the optimizations of S_1, time dependent density functional theory (TD-DFT)[25] is adopted to obtain the computation of emission energies, oscillator strengths, and composition of excited states in terms of singly excited Slater determinants. Bond lengths and dihedral angles obtained from B3LYP/6-31G(d) S_0 and CIS/6-31G(d) S_1 are summarized in Table S1 (ESI†), with the atoms denoted by numbers in Fig. S2 (ESI†). The geometrical variations between B3LYP/6-31G(d) S_0 and CIS/6-31G(d) S_1 in the dihedral angles $\Phi(16,1,17,18)$ of **TICCBI** increased from 52° to 55°, whereas **TICNBI** showing a greater rotation from 53.8° to 68.4° was observed. These results indicate that the molecular configuration of indolocarbazole (D) and benzimidazole (A) in **TICNBI** twists in S_1 with poor coplanarity, which agrees with the lack of D to A charge transfer behaviour in the previous solvent-dependent emission experiments.

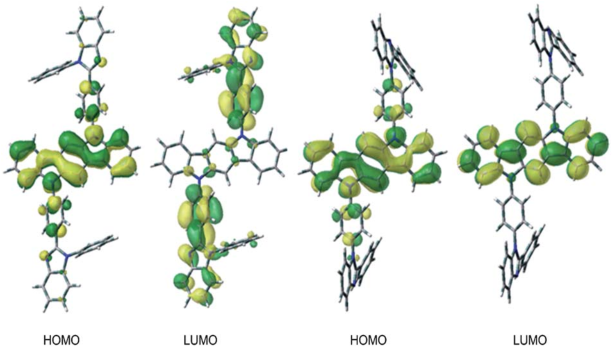

Fig. 2 S_0 frontier molecular orbitals (HOMO and LUMO) of **TICCBI** (left) and **TICNBI** (right), calculated with DFT at a B3LYP/6-31G (d) level.

The calculated first electronic transitions, emission wavelengths, oscillator strengths (*f*), composition in terms of molecular orbital configurations and experimental emissions are listed in Table 2. Decisive evidence was given combining the results of Table 2 and Fig. 2, the emission peak with larger oscillator strength of **TICCBI** at 396.8 nm was assigned as a D–A charge transfer character, arising from the indolocarbazole-centered HOMO to the benzimidazole-located LUMO. In contrast, the smaller oscillator strength of HOMO → LUMO transition of **TICNBI** indicates no relevance to the D–A charge transfer. Computational analyses for the excited-state geometries and electronic transitions confirmed experimental emission spectra where obvious D–A charge transfer character in **TICCBI** was shown. We are convinced with theoretical tools, it is possible to reasonably investigate the electronic characteristics of structure-similar systems and provide insights to clearly define the structure–properties relation.

2.5 Electrochemical properties

The electrochemical properties of **TICCBI** and **TICNBI** were examined by cyclic voltammetry (CV) (Fig. 3). The observed reversible oxidation potential and quasi-reversible reduction potential in **TICCBI** can be ascribed to the indolocarbazole and *N*-phenylbenzimidazole, respectively. It is interesting to see the difference in the oxidation potentials of **TICCBI** and **TICNBI**, where, **TICCBI** exhibited a lower oxidation potential owing to the slightly extended π-conjugation of indolocarbazole through C-connectivity to *N*-phenylbenzimidazole. As compared to **TICCBI**, the reduction of **TICNBI** shows poor reversibility, which is because the LUMO is localized on the electron-rich central indolocarbazole as shown in the theoretical calculation. It is intriguing to note that electropolymerization did not occur during multiple-cycle CV scans (Fig. S3 in the ESI†), implying superior electrochemical stability of **TICCBI** and **TICNBI** as compared to those of carbazole-based materials. We believe that the radical cations of **TICCBI** and **TICNBI** upon electrochemical oxidation are localized on the central phenylene ring of the indolocarbazole core, impeding efficient electropolymerization. Thus, the appending of the electron-transporting *N*-phenylbenzimidazole units onto the indolocarbazole core renders **TICCBI** and **TICNBI** with promising electrochemical stability, bipolar characteristics and their potential for efficient hole and electron transport. The HOMO energy levels of **TICCBI** and **TICNBI** were determined using photoelectron yield spectroscopy (Riken AC-2), and the LUMO energy levels were calculated from the HOMO values by using the equation LUMO = HOMO + E_g, where E_g is the optical band gap determined from the onset wavelength of the absorption band. The calculated HOMO/LUMO energies are summarized in Table 1.

Table 2 Calculated emission data derived from TDDFT//B3LYP/6-31G(d) according to the CIS/6-31G(d) optimized geometries

Host	Electronic transition	λ_{em}/nm	f	MO configuration	Coefficient	Exp. λ_{em}/nm
TICCBI	$S_1 \rightarrow S_0$	396.8	0.69	HOMO → LUMO	0.7	439
TICNBI	$S_1 \rightarrow S_0$	377	0.13	HOMO → LUMO	0.61	435
—	—	—	—	HOMO − 1 → LUMO	0.32	—

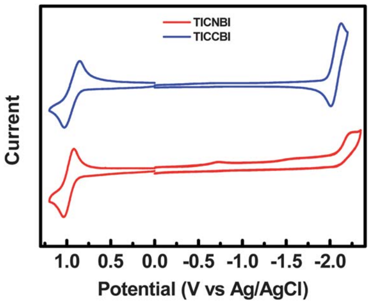

Fig. 3 Cyclic voltammograms of **TICCBI** and **TICNBI**; 0.1 M TBAP (reduction) in DMF and 0.1 M TBAPF$_6$ (oxidation) in CH$_2$Cl$_2$ were used as supporting electrolytes. A glassy carbon electrode was used as the working electrode; scan rate: 100 mV s^{-1}.

2.6 Crystal structure

In order to get better idea of intermolecular interactions of **TICCBI** and **TICNBI**, suitable single crystals of **TICNBI** were obtained by sublimation, whereas crystals of **TICCBI** were obtained by slow evaporation of the DMSO solvent. X-Ray diffraction analyses indicate that we get the crystals of **TICCBI** and **TICNBI** packed in the monoclinic crystal structure with space group $P2_1/n$ and triclinic crystal structure with space group $P1$, respectively (Table S2 in the ESI†). In **TICCBI**, the dihedral angles between indolocarbazole/phenylene-linker and phenylene-linker/benzimidazole were calculated as 52.8° and 56.3°, respectively, whereas in **TICNBI**, the dihedral angles were calculated as 32.6° and 59.6°, respectively. The highly twisted conformations render the molecules rather bulky and in noncoplanar conformation as shown in Fig. 4. The noncoplanar molecular conformation prevents the intermolecular interaction which enables them to form amorphous thin film *via* vacuum deposition. The crystal packing of **TICCBI** indicates the absence of intermolecular π–π interactions, in which the closest plane-to-plane distance between benzimidazole and phenylene linker was estimated to be *ca.* 4.3 Å. In contrast, the crystal packing of **TICNBI** shows interesting intermolecular D–A interactions, in which the closest plane-to-plane distance between benzimidazole and central indolocarbazole was estimated to be *ca.* 3.8 Å (Fig. 4).

2.7 Charge carrier mobility and electron only devices

In order to confirm the hypothesis that the appending of electron-accepting *N*-phenylbenzimidazole units onto the electron-donating indolo-carbazole core renders **TICCBI** and **TICNBI** with promising bipolar transporting nature, we used time-of-flight (TOF) techniques to measure carrier mobility.[26] The device used for TOF measurement was prepared through vacuum deposition with the structure ITO–glass/**TICCBI** (1.8 μm) or **TICNBI** (2.3 μm)/Ag (150 nm) and then it was placed inside a cryostat under vacuum. Fig. 5(a) and (b) show the representative TOF transient for holes. Both transient photocurrent signals were dispersive, suggesting the presence of hole traps. The transit time, t_T, can be evaluated from the intersection point of two asymptotes in the double-logarithmic representation of the TOF transient. It needed to determine the carrier mobilities according to the equation $\mu = d^2/Vt_T$, where d is the sample thickness and V is the applied voltage. Fig. 5(c) shows the field dependence of the hole mobility follows the nearly universal Poole–Frenkel relationship and the values are in the range of 4×10^{-6} to 2×10^{-5} cm^2 V^{-1} s^{-1} for **TICCBI** and 1×10^{-5} to 4×10^{-5} cm^2 V^{-1} s^{-1} for **TICNBI** at fields varying from 2.6×10^5 to 5.5×10^5 V cm^{-1}. In contrast, the electron transient photocurrent signals were too weak, which cannot be used to determine the electron mobility by the TOF technique.

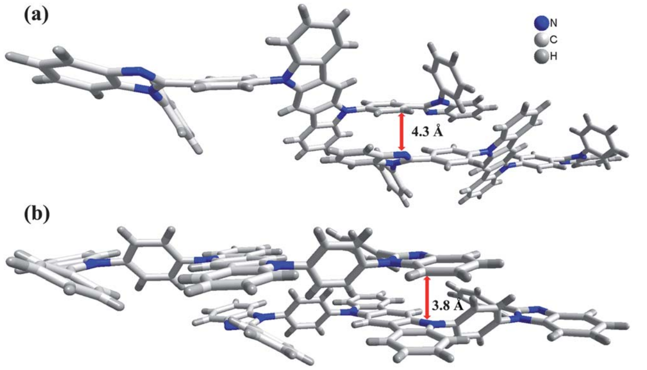

Fig. 4 Crystal packing of (a) **TICCBI** and (b) **TICNBI**. The solvent molecules are omitted for clarity.

For the assessment of electron transport property, the electron-only device was fabricated with a device structure of ITO/BCP (30 nm)/**TICCBI** or **TICNBI** (50 nm)/TPBI (20 nm)/LiF/Al. Here, BCP serves as the hole-blocking layer to impede the hole current in the device. Fig. 6 depicts the current *vs.* voltage characteristics of electron-only devices. The introduction of BCP contacting to ITO is for limiting the injection of hole carrier, as shown in the inset of Fig. 6. Apparently, different linking topologies (C- or N-connection of benzimidazole) have pronounced effect on the electron transport and the magnitude of current follows the order: **TICCBI > TICNBI**.

2.8 OLED device

To investigate the new indolocarbazole–benzimidazole hybrid materials (**TICCBI** and **TICNBI**) as hosts in organic light emitting diodes, we fabricated the emitting device with typical multi-layer architecture of indium-tin-oxide (ITO)/polyethylene dioxythiophene:polystyrene sulfonate (PEDOT:PSS, 30 nm)/4,4′-bis[*N*-(1-naphthyl)-*N*-phenyl-amino]biphenyl (NPB, 20 nm)/4,4′,4″-tri(*N*-carbazolyl)triphenylamine (TCTA, 5 nm)/emitter

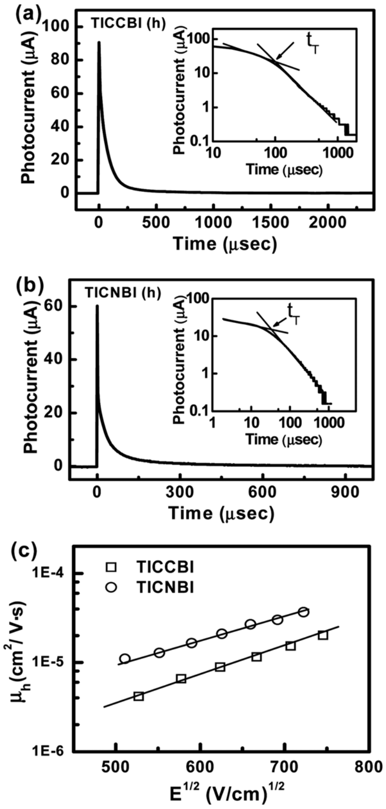

Fig. 5 Representative TOF transients for (a) **TICCBI** (1.8 μm thickness; $E = 3.3 \times 10^5$ V cm^{-1}); (b) **TICNBI** (2.3 μm thickness; $E = 3.9 \times 10^5$ V cm^{-1}). Inset: double-logarithmic plot. (c) Hole mobilities of **TICCBI** and **TICNBI** plotted with respect to $E^{1/2}$.

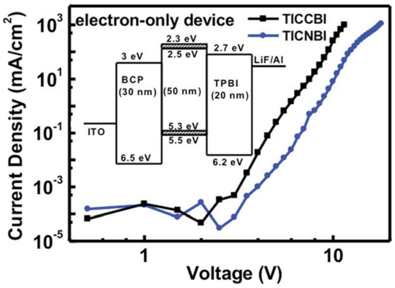

Fig. 6 Current density–voltage (*I–V*) characteristics of electron-only devices.

(25 nm)/1,3,5-tris(*N*-phenylbenzimidizol-2-yl)benzene (TPBI, 50 nm)/LiF (0.5 nm)/Al (100 nm), for which the hosts are **TICCBI** for device **A**, or **TICNBI** for device **B**. Among the numerous possible heavy-metal containing complexes, we chose the bis(2-phenylpyridinato) iridium(III) acetylacetonate $(PPy)_2Ir(acac)$[27] for green emission, bis(2-phenyl benzothiozolato-N,C$^{2'}$) iridium (acetylacetonate) $(Bt)_2Ir(acac)$[28] for yellow emission and osmium(II) bis(3-(trifluoromethyl)-5-(4-*tert*-butylpyridyl)-1,2,4-triazolate) dimethylphenylphosphine $Os(bpftz)_2(PPhMe_2)_2$,[29] as well as $(35dmPh\text{-}6Fiq)_2Ir(acac)$ (**i3**) and $(4t\mathrm{BuPh}\text{-}6Fiq)_2Ir(acac)$ (**i6**) for red emissions. The doping concentration of the dopants is 10 wt%. NPB was used as the hole-transporting layer, TPBI was used as the electron-transporting layer, and LiF and Al were used as the electron injecting layer and cathode, respectively. Moreover, a thin layer (*ca.* 5 nm) of TCTA was inserted between NPB and the emitting layer (EML) to reduce the excessive energy barrier between NPB and the host material. Scheme 2 shows chemical structures of the heavy metal containing complexes used in this study.

The current density–voltage–luminance (*J–V–L*) characteristics, external quantum efficiency as well as power efficiency *versus* luminance curve, and EL spectra of the devices are shown in Fig. 7 and 8. All the device performances are summarized in Table 3.

All turn-on voltages of the **TICCBI**-based devices (2 eV) are lower than those of the **TICNBI**-based devices (2.5 eV), which could be attributed to the HOMO level of **TICCBI** (−5.3 eV) which is 0.2 eV higher than that of **TICNBI** (−5.5 eV). Taking the difference in the *J–V* performance caused by using different emitting dopant into account, we could make a conclusion that the emitting dopants could have a strong influence on the charge carrier transport of the emission layer. We initially examined the performance of $(PPy)_2Ir(acac)$-based green devices (devices **A1** and **B1**). Fig. 7(a) shows that the *J–V–L* characteristics of devices **A1** and **B1** are nearly identical, indicating that hosts **TICCBI** and **TICNBI** have very little influence on the charge transport characteristics and the driving voltage is approximately 5.6 and 5.1 V at 1000 cd m^{-2}, respectively. As shown in Fig. 7(b), the device **B1** using **TICNBI** host exhibited the higher external quantum efficiency (η_{ext}) of 15%, current efficiency (η_c) of 55.8 cd A^{-1} and power efficiency (η_p) of 56 lm W^{-1} as compared with that (14%, 52.4 cd A^{-1}, and 31.2 lm W^{-1}) of device **A1** using **TICCBI** as the host. It is worth noting that the η_{ext} of device **B1** still remains as high as 14.9% at a brightness of 1000 cd m^{-2} without significant decay, which can be explained by the balance of charge carriers in the emitting layer. Next, we fabricated yellow phosphorescent devices (devices **A2** and **B2**) using $(Bt)_2Ir(acac)$ as the dopant. As the green devices, the device **B2** incorporating **TICNBI** as the host exhibited higher efficiencies (16.2%, 45.7 cd A^{-1}, and 37 lm W^{-1}) relative to that of device **A2** (15.4%, 42.2 cd A^{-1}, and 31.6 lm W^{-1}). These values are comparable with those of yellow phosphorescent devices in the literature,[30] which may serve as the potential emitting element for generating white light in combination with a complementary blue phosphor.[31]

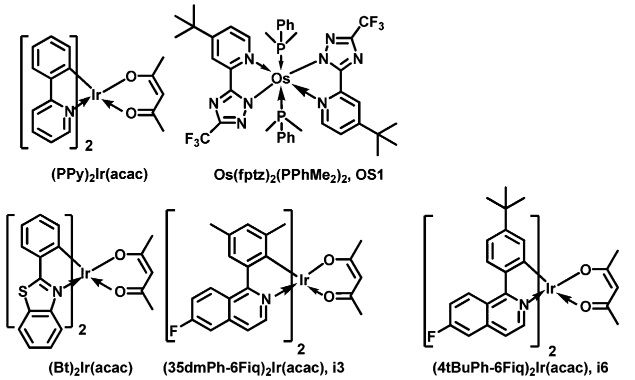

Scheme 2 Chemical structures of the heavy metal complex used in this study.

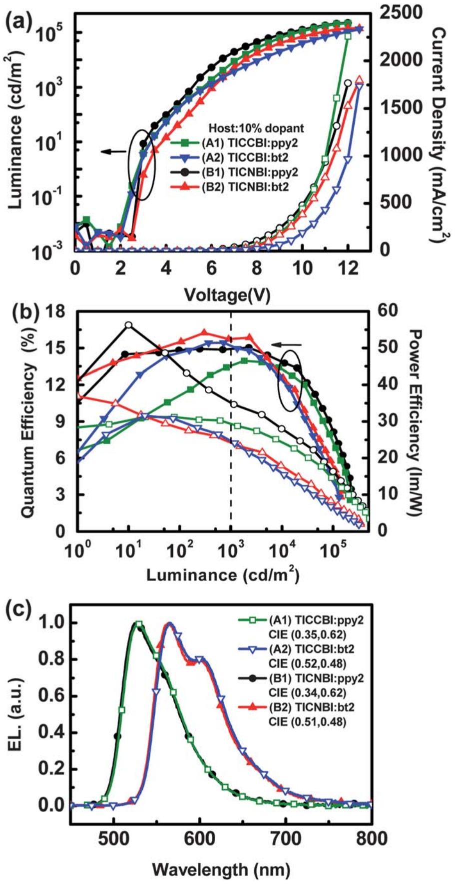

Fig. 7 (a) *L–V–J* characteristics, (b) plots of EL efficiency *versus* brightness and (c) EL spectra for devices incorporating **TICCBI** and **TICNBI** doped with 10 wt% $PPy_2Ir(acac)$ and $Bt_2Ir(acac)$.

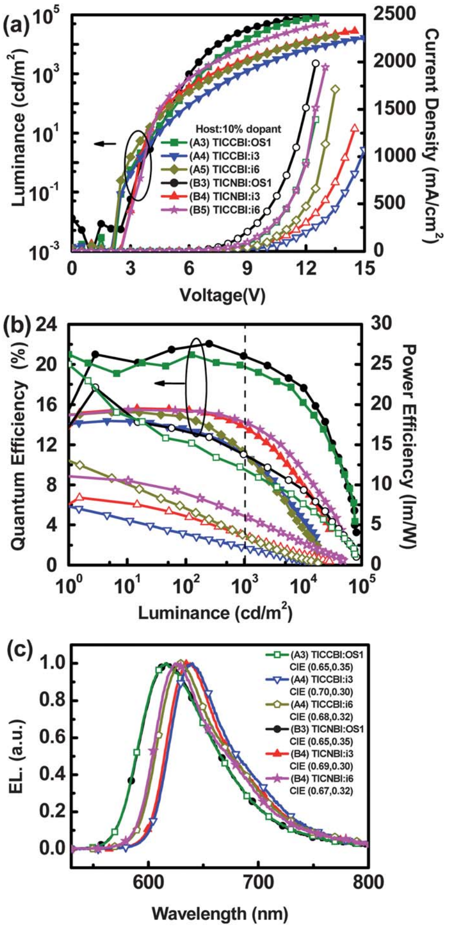

Fig. 8 (a) *L–V–J* characteristics, (b) plots of EL efficiency *versus* brightness and (c) EL spectra for devices incorporating **TICCBI** and **TICNBI** doped with 10 wt% Os1, $(35dmPh\text{-}6Fiq)_2Ir(acac)$ (**i3**) and $(4tBuPh\text{-}6Fiq)_2Ir(acac)$ (**i6**).

Finally, we demonstrated highly efficient red phosphorescent devices using the emitters composed of the third-row Os(II) (devices **A3** and **B3**) and phenylisoquinolinyl chelated Ir(III) (devices **A4**, **A5**, **B4** and **B5**) complexes. The device characteristics are shown in Fig. 8 and data are summarized in Table 3. The devices exhibited relatively pure red emission with the corresponding CIE (Commission Internationale de L'éclairage) coordinates $x = 0.65$, $y = 0.35$ for $Os(bpftz)_2(PPhMe_2)_2$ and $x = 0.67\text{–}0.70$, $y = 0.30\text{–}0.32$ for phenylisoquinolinyl-Ir(III), respectively. The best EL performance is achieved for device **B3** with $Os(bpftz)_2(PPhMe_2)_2$ doped in **TICNBI**, in which very high η_{ext} of 22%, η_c of 28 cd A^{-1}, and η_p of 22.1 lm W^{-1} were obtained, whereas the η_{ext} still remains 20.8% at 1000 cd m^{-2}. Compared to contemporary results, device **B3** is the best of Os-based devices.[29,32] For device **A3** using **TICCBI** as host, the device performance also achieved 21%, 26.6 cd A^{-1}, and 25 lm W^{-1},

Table 3 Electroluminescent properties of the devices

Device	Host: 10% dopant	$V_{on}{}^a$/ V	At 1000 nit^b/ V, %	L_{max}/ cd m^{-2}	I_{max}/ mA cm^{-2}	η_{ext} max/ %, cd A^{-1}	η_p max/ lm W^{-1}	CIE1931 (x,y)
A1	**TICCBI**: $PPy_2Ir(acac)$	2	5.6, 13.5	218 400 (12 V)	2260	14, 52.4	31.2	0.35,0.62
A2	**TICCBI**: $Bt_2Ir(acac)$	2	5.7, 15.2	132 600 (12.5 V)	1740	15.4, 42.2	31.6	0.52,0.48
A3	**TICCBI**: Os1	2	6.6, 20	76 900 (12.5 V)	1400	21, 26.6	25	0.65,0.35
A4	**TICCBI**: $(35dmPh\text{-}6Fiq)_2Ir(acac)$	2	8.7, 11	16 900 (15.5 V)	1440	14.4, 7.9	8	0.70,0.30
A5	**TICCBI**: $(4tBuPh\text{-}6Fiq)_2Ir(acac)$	2	7.6, 11	18 100 (13.5 V)	1710	15.3, 12	13	0.68,0.32
B1	**TICNBI**: $PPy_2Ir(acac)$	2.5	5.1, 14.9	225 600 (12 V)	1770	15, 55.8	56	0.34,0.62
B2	**TICNBI**: $Bt_2Ir(acac)$	2.5	6, 15.7	142 300 (12.5 V)	1800	16.2, 45.7	37	0.51,0.48
B3	**TICNBI**: Os1	2.5	6, 20.8	81 600 (12.5 V)	1990	22, 28	22.1	0.65,0.35
B4	**TICNBI**: $(35dmPh\text{-}6Fiq)_2Ir(acac)$	2.5	7.2, 13.6	28 300 (14.5 V)	1300	15.6, 9.6	8.4	0.69,0.30
B5	**TICNBI**: $(4tBuPh\text{-}6Fiq)_2Ir(acac)$	2.5	6.4, 14.2	48 300 (13 V)	1940	15.5, 13.4	10.5	0.67,0.32

^{a} Turn-on voltage at which emission became detectable. ^{b} The values of driving voltage and η_{ext} of device at 1000 cd m^{-2}.

whereas the η_{ext} still remains 20% at 1000 cd m^{-2}. Considering the out coupling factor, this is reaching nearly 100% internal efficiency. The high efficiency and low efficiency roll-off at high luminance for devices **A3** and **B3** can be attributed to the use of the bipolar hosts **TICCBI** and **TICNBI**, which may have resulted in balanced charge fluxes and a broad distribution of recombination region within the emitting layer. For devices **A4** and **B4** doped with (35dmPh-6Fiq)$_2$Ir(acac), they displayed deep-red emission with CIE coordinates of (0.70,0.30) and the device performances (14.4–15.6%). For devices **A5** and **B5** doped with (4*t*BuPh-6Fiq)$_2$Ir(acac), they displayed deep-red emission with CIE coordinates of (0.68,0.32) and the device performances (15.3–15.5%) are significantly better than those of phenylisoquinolinyl-iridium complexes using CBP as the host.[33]

By altering the linking topology (C- or N-connectivity) of the benzimidazole substituents at the central indolo-carbazole core, the efficiencies of the devices based on **TICNBI** as host are typically higher than those based on **TICCBI**, which may be due to the superior carrier balance that caused greater degree of energy transfer in the emissive layer. These findings show that even small structural variations may change the charge-carrier balance in the device or the chemical compatibility of host and emitter. This information could be useful for the design of an efficient host.

Conclusions

Two new bipolar host materials **TICCBI** and **TICNBI** composed of indolo[3,2-*b*]carbazole donor core and *N*-phenyl benzimidazole acceptor peripherals were designed and synthesized. The physical properties of the hosts can be modulated through the different linkages between the electronic donor and acceptor components. The promising properties include reversible redox behavior, high morphological stability, and suitable energy levels, rendering them as potential good candidates for realizing highly efficient eletrophosphorescence devices. PhOLEDs incorporating **TICCBI** as the host doped with Ir-based emitters such as green (PPy)$_2$Ir(acac), yellow (Bt)$_2$Ir(acac), and two new red emitters (35dmPh-6Fiq)$_2$Ir(acac) (**i3**) and (4*t*BuPh-6Fiq)$_2$Ir(acac) (**i6**) accomplished high external quantum efficiencies ranging from 14 to 15.3%. In contrast, the devices hosted by **TICNBI** achieved the best EL performance, with a maximum current efficiency (η_c) of 28 cd A^{-1} and maximum external quantum efficiency (η_{ext}) of 22% for Os-based red electrophosphorescence, 55.8 cd A^{-1} and 15% for green electrophosphorescence, and 45.7 cd A^{-1} and 16.2% for yellow electrophosphorescence. The η_{ext} remains as high as 20% for red and 14.9% for green electrophosphorescence at a brightness of 1000 cd m^{-2}. The high efficiency and low efficiency roll-off at high luminance can be attributed to the balanced charge fluxes, a broad distribution of recombination region within the emitting layer, the well-matched energy levels between the host and hole-transport layer, and complete spatial separation of HOMO and LUMO energy levels. The EL performances of the devices closely correlate to the molecular structural features, and substantial gains in the EL performances can be made by subtle changes in the design of the host material. Our study presents a new guideline for the molecular design of amorphous bipolar materials, paving the way for the development of next generation amorphous bipolar host molecules for PhOLEDs.

Acknowledgements

We greatly appreciate the financial support from National Science Council of Taiwan (NSC 98-2119-M-002-007-MY3 and 100-2112-M-019-002-MY3) and Ministry of Economic Affairs (100-EC-17-A-08-S1-042).

Notes and references

1 (*a*) C. W. Tang and S. A. VanSlyke, *Appl. Phys. Lett.*, 1987, **51**, 913; (*b*) M. A. Baldo, M. E. Thompson and S. R. Forrest, *Nature*, 2000, **403**, 750.

2 M. A. Baldo, D. F. O'Brien, Y. You, A. Shoustikov, S. Sibley, M. E. Thompson and S. R. Forrest, *Nature*, 1998, **395**, 151.

3 S.-J. Su, H. Sasabe, T. I. Takeda and J. Kido, *Chem. Mater.*, 2008, **20**, 1691.

4 H. H. Fong, C. H. Wallace Choy, K. N. Hui and Y. J. Liang, *Appl. Phys. Lett.*, 2006, **88**, 113510.

5 (*a*) C. Adachi, R. C. Kwong, P. Djurovich, V. Adamovich, M. A. Baldo, M. E. Thompson and S. R. Forrest, *Appl. Phys. Lett.*, 2001, **79**, 2082; (*b*) R. J. Holmes, S. R. Forrest, Y.-J. Tung, R. C. Kwong, J. J. Brown, S. Garon and M. E. Thompson, *Appl. Phys. Lett.*, 2003, **82**, 2422; (*c*) S. Tokito, T. Iijima, Y. Suzuri, H. Kita, T. Tsuzuki and F. Sato, *Appl. Phys. Lett.*, 2003, **83**, 569; (*d*) K. Goushi, R. Kwong, J. J. Brown, H. Sasabe and C. Adachi, *J. Appl. Phys.*, 2004, **95**, 7798.

6 (*a*) M. A. Baldo, S. Lamansky, P. E. Burrows, M. E. Thompson and S. R. Forrest, *Appl. Phys. Lett.*, 1999, **75**, 4; (*b*) M. H. Lu, M. S. Weaver, T. X. Zhou, M. Rothman, R. C. Kwong, M. Hack and J. J. Brown, *Appl. Phys. Lett.*, 2002, **81**, 3921.

7 (*a*) A. Chaskar, H.-F. Chen and K.-T. Wong, *Adv. Mater.*, 2011, **23**, 3876; (*b*) S. O. Jeon, S. E. Jang, H. S. Son and J. Y. Lee, *Adv. Mater.*, 2011, **23**, 1436; (*c*) Y. Tao, Q. Wang, C. Yang, C. Zhong, J. Qin and D. Ma, *Adv. Funct. Mater.*, 2010, **20**, 2923.

8 (*a*) S. Gong, Y. Chen, J. Luo, C. Yang, C. Zhong, J. Qin and D. Ma, *Adv. Funct. Mater.*, 2011, **21**, 1168; (*b*) S. Gong, Y. Chen, C. Yang, C. Zhong, J. Qin and D. Ma, *Adv. Mater.*, 2010, **22**, 5370.

9 H.-H. Chou and C.-H. Cheng, *Adv. Mater.*, 2010, **22**, 2468.

10 W.-Y. Hung, L.-C. Chi, W.-J. Chen, Y.-M. Chen, S.-H. Chou and K.-T. Wong, *J. Mater. Chem.*, 2010, **20**, 10113.

11 Y. Tao, C. Yang and J. Qin, *Chem. Soc. Rev.*, 2011, **40**, 2943.

12 Y. Wu, Y. Li, S. Gardner and B. S. Ong, *J. Am. Chem. Soc.*, 2005, **127**, 614.

13 (*a*) N. X. Hu, S. Xie, Z. Popovic, B. Ong and A. M. Hor, *J. Am. Chem. Soc.*, 1999, **121**, 5097; (*b*) H. P. Zhao, X. T. Tao, P. Wang, Y. Ren, J. X. Yang, Y. X. Yan, C.-X. Yuan, H. J. Liu, D. C. Zou and M. H. Jiang, *Org. Electron.*, 2007, **8**, 673; (*c*) S. Lengvinaite, J. V. Grazulevicius, S. Grigalevicius, R. Gu, W. Dehaen, V. Jankauskas, B. Zhang and Z. Xie, *Dyes Pigm.*, 2010, **85**, 183.

14 (*a*) P. T. Boudreault, S. Wakim, M. L. Tang, Y. Tao, Z. Bao and M. Leclerc, *J. Mater. Chem.*, 2009, **19**, 2921; (*b*) Y. Guo, H. Zhao, G. Yu, C. Di, W. Liu, S. Jiang, S. Yan, C. Wang, H. Zhang, X. Sun, X. Tao and Y. Liu, *Adv. Mater.*, 2008, **20**, 4835.

15 (*a*) J. Lu, F. Liang, N. Drolet, J. Ding, Y. Tao and R. Movileanu, *Chem. Commun.*, 2008, 5315; (*b*) E. Zhou, S. Yamakawa, Y. Zhang, K. Tajima, C. Yanga and K. Hashimoto, *J. Mater. Chem.*, 2009, **19**, 7730.

16 S. Lengvinaite, J. V. Grazulevicius, S. Grigalevicius, R. Gu, W. Dehaen, V. Jankauskas, B. Zhang and Z. Xie, *Dyes Pigm.*, 2010, **85**(3), 183.

17 (*a*) Y.-J. Su, H.-L. Huang, C.-L. Li, C.-H. Chien, Y.-T. Tao, P.-T. Chou, S. Datta and R.-S. Liu, *Adv. Mater.*, 2003, **15**, 884; (*b*) C. L. Li, Y. J. Su, Y. T. Tao, P. T. Chou, S. Datta and R. S. Liu, *Adv. Funct. Mater.*, 2005, **15**, 387.

18 (*a*) V. V. Grushin, N. Herron, D. D. LeCloux, W. J. Marshall, V. A. Petrov and Y. Wang, *Chem. Commun.*, 2001, 1494; (*b*) Y. Wang, N. Herron, V. V. Grushin, D. LeCloux and V. Petrov, *Appl. Phys. Lett.*, 2001, **79**, 449.

19 (*a*) I. R. Laskar and T.-M. Chen, *Chem. Mater.*, 2004, **16**, 111; (*b*) K.-H. Fang, L.-L. Wu, Y.-T. Huang, C.-H. Yang and I.-W. Sun, *Inorg. Chim. Acta*, 2006, **359**, 441; (*c*) C.-H. Yang, C.-C. Tai and I.-W. Sun, *J. Mater. Chem.*, 2004, **14**, 947; (*d*) P. J. Hay, *J. Phys. Chem. A*, 2002, **106**, 1634.

20 L. N. Yudina and J. Bergman, *Tetrahedron*, 2003, **59**, 1265.

21 Z. Ge, T. Hayakawa, S. Ando, M. Ueda, T. Akiike, H. Miyamoto, T. Kajita and M.-A. Kakimoto, *Adv. Funct. Mater.*, 2008, **18**, 584.

22 F.-M. Hsu, C.-H. Chien, C.-F. Shu, C.-H. Lai, C.-C. Hsieh, K.-W. Wang and P.-T. Chou, *Adv. Funct. Mater.*, 2009, **19**, 2834.

23 Y. L. Liu, J. K. Feng and A. M. Ren, *J. Phys. Chem. A*, 2008, **112**, 3157.

24 R. J. Cave, K. Burke and E. W. Castner, Jr, *J. Phys. Chem. A*, 2002, **106**, 9294.

25 M. E. Casida, C. Jamorski, K. C. Casida and D. R. Salahub, *J. Chem. Phys.*, 1998, **108**, 4439.

26 M. Borsenberger and D. S. Weiss, in *Organic Photoreceptors for Imaging Systems*, New York, 1993, and references therein.

27 C. Adachi, M. A. Baldo, M. E. Thompson and S. R. Forrest, *J. Appl. Phys.*, 2001, **90**, 5048.

28 (*a*) S. Lamansky, P. Djurovich, D. Murphy, F. Abdel-Razzaq, H.-E. Lee, C. Adachi, P. E. Burrows, S. R. Forrest and M. E. Thompson, *J. Am. Chem. Soc.*, 2001, **123**, 4304; (*b*) W.-C. Chang, A. T. Hu, J.-P. Duan, D. K. Rayabarapu and C.-H. Cheng, *J. Organomet. Chem.*, 2004, **689**, 4882.

29 Y.-L. Tung, S.-W. Lee, Y. Chi, Y.-T. Tao, C.-H. Chien, Y.-M. Cheng, P.-T. Chou, S.-M. Peng and C.-S. Liu, *J. Mater. Chem.*, 2005, **15**, 460.

30 (*a*) C.-L. Ho, W.-Y. Wong, Q. Wang, D. Ma, L. Wang and Z. Lin, *Adv. Funct. Mater.*, 2008, **18**, 928; (*b*) Y.-S. Park, J.-W. Kang, D. M. Kang, J.-W. Park, Y.-H. Kim, S.-K. Kwon and J.-J. Kim, *Adv. Mater.*, 2008, **20**, 1957; (*c*) W.-Y. Hung, L.-C. Chi, W.-J. Chen, Y.-M. Chen, S.-H. Chou and K.-T. Wong, *J. Mater. Chem.*, 2010, **20**, 10113; (*d*) S.-L. Lai, S.-L. Tao, M.-Y. Chan, M.-F. Lo, T.-W. Ng, S.-T. Lee, W.-M. Zhao and C.-S. Lee, *J. Mater. Chem.*, 2011, **21**, 4983; (*e*) R. Wang, D. Liu, H. Ren, T. Zhang, H. Yin, G. Liu and J. Li, *Adv. Mater.*, 2011, **23**, 2823.

31 H. Sasabe, J. Takamatsu, T. Motoyama, S. Watanabe, G. Wagenblast, N. Langer, O. Molt, E. Fuchs, C. Lennartz and J. Kido, *Adv. Mater.*, 2010, **22**, 5003.

32 (*a*) C.-H. Chien, F.-M. Hsu, C.-F. Shu and Y. Chi, *Org. Electron.*, 2009, **10**, 871; (*b*) S.-Y. Ku, W.-Y. Hung, C.-W. Chen, S.-W. Yang, E. Mondal, Y. Chi and K.-T. Wong, *Chem.–Asian J.*, 2012, **7**, 133.

33 (*a*) H.-C. Li, P.-T. Chou, Y.-H. Hu, Y.-M. Cheng and R.-S. Liu, *Organometallics*, 2005, **24**, 1331; (*b*) Y.-J. Su, H.-L. Huang, C.-L. Li, C.-H. Chien, Y.-T. Tao, P.-T. Chou, S. Datta and R.-S. Liu, *Adv. Mater.*, 2003, **15**, 884; (*c*) C.-L. Li, Y.-J. Su, Y.-T. Tao, P.-T. Chou, C.-H. Chien, C.-C. Cheng and R.-S. Liu, *Adv. Funct. Mater.*, 2005, **15**, 387.